Published in final edited form as:
Geochim Cosmochim Acta. 2019 April 15; 251: 217–228. doi:10.1016/j.gca.2019.02.035.

Genetics, crystallization sequence, and age of the South Byron Trio iron meteorites: New insights to carbonaceous chondrite (CC) type parent bodies

Connor D. Hilton[1], **Katherine R. Bermingham**[1], **Richard J. Walker**[1], **Timothy J. McCoy**[2]

[1]Department of Geology, University of Maryland, College Park, Maryland, 20742, USA

[2]Department of Mineral Sciences, National Museum of Natural History, Smithsonian Institution, Washington, DC, 20560-0119, USA

Abstract

The nucleosynthetic Mo, Ru, and W isotopic compositions of the South Byron Trio iron meteorite grouplet (SBT) are consistent with all three meteorites originating on a single parent body that formed in the carbonaceous chondrite (CC) isotopic domain within the Solar nebula. Consistent with a common origin, the highly siderophile element (HSE) concentrations of the SBT can be related to one another by moderate degrees of fractional crystallization of a parental melt with initially chondritic relative abundances of HSE, and with initial S and P contents of ~7 and ~1 wt. %, respectively. Tungsten-182 isotopic data for the SBT indicate the parent body underwent metal-silicate differentiation 2.1 ± 0.8 Myr after calcium aluminum rich inclusion formation, and thermal modeling suggests the parent body formed 1.1 ± 0.5 Myr after CAI formation. This accretion age is not resolved from the accretion ages of other CC and most noncarbonaceous (NC) type iron meteorite parent bodies. Comparison of the projected parental melt composition of the SBT to those projected for the IVA and IVB iron meteorite groups suggests that at least some portions of the CC nebular domain were more oxidized compared to the NC domain. In addition, comparison of the SBT parental melt S content to estimates for parent bodies of the IIAB, IIIAB, IVA, IID, and IVB “magmatic” iron meteorite groups suggests that CC type iron meteorite parental melts were characterized by a general depletion in S, in addition to depletions in some other moderately volatile elements.

Based on chemical and O isotope similarities, prior studies have suggested the possibility of a common parent body for the SBT and the Milton pallasite. Molybdenum and Ru isotopic compositions of Milton also provide permissive evidence for this. The HSE concentrations in the Milton metal, however, cannot be related to the SBT by any known crystal-liquid fractionation or mixing path. Thus, Milton more likely formed on a different, chemically distinct, but genetically identical parent body present in the CC nebular domain.

Keywords

Accretion age; Fractional crystallization; Nucleosynthesis; Hf-W chronometry; Iron meteorites; Pallasite

chilton@umd.edu.

1. Introduction

Two isotopically and likely chemically distinct nebular domains, referred to as "noncarbonaceous" (NC) and "carbonaceous" (CC), were originally identified to have existed in the early Solar System through studies of Ni, Cr, Ti, and O isotopic compositions in meteorites (Warren, 2011). The list of isotopically diverse elements to discriminate between these domains has been expanded to include the siderophile elements Mo, Ru, and W, which allow for the NC and CC classification to be extended to iron meteorites and pallasite metal (e.g., Fisher-Gödde et al., 2015; Budde et al., 2016; Kruijer et al., 2017; Poole et al., 2017; Worsham et al., 2017; Bermingham et al., 2018). Mass independent isotopic heterogeneity observed for Mo, Ru, and W among early Solar System materials is due to the incorporation of variable proportions of presolar components with isotopically diverse compositions reflecting different nucleosynthetic origins (e.g., Dauphas et al., 2002; Qin et al., 2008; Chen et al., 2010). The distinct Mo, Ru, and W isotopic compositions of the NC and CC isotopic domains have been interpreted to represent the division and isolation of the inner and outer Solar System, possibly due to the formation of proto-Jupiter (Warren, 2011; Budde et al., 2016; Kruijer et al., 2017). As the outer Solar System is expected to be a more oxidizing and volatile-rich environment compared to the inner Solar System, coupled studies of isotopic and chemical compositions of CC type iron meteorites may provide new insights into the NC and CC division, and nebular heterogeneity.

So called "magmatic" iron meteorite groups consist of multiple meteorites whose chemical differences can be accounted for by crystal-liquid fractionation and mixing processes originating from a single melt. Most of the major magmatic iron meteorite groups have been characterized as NC or CC based on Mo, Ru, and W isotopic compositions. The NC type irons include the IC, IIAB, IIIAB, IIIE, and IVA groups, and the CC type irons include the IIC, IID, IIF, IIIF, and IVB groups (Fisher-Gödde et al., 2015; Budde et al., 2016; Kruijer et al., 2017; Poole et al., 2017; Worsham et al., 2017; Bermingham et al., 2018). Of these ten iron groups, the CC type irons tend toward greater Ni contents and more limited ranges in Ir concentrations compared to NC irons, although there is considerable overlap (Fig. 1). Additional chemical comparisons between NC and CC type iron meteorites are limited. For example, the highly siderophile element (HSE; Re, Os, Ir, Ru, Pt, Pd) concentrations of parental melts have only been estimated for the IVA and IVB iron meteorites (Campbell and Humayun, 2005; Walker et al., 2008; McCoy et al., 2011). In addition, S contents of iron meteorite parental melts have been determined using multiple approaches that are not always consistent, limiting direct comparisons (e.g., Chabot, 2004; Wasson et al., 2007).

The South Byron Trio (SBT) iron meteorite grouplet provides an opportunity to expand knowledge regarding the chemical and isotopic variability of the Solar nebula. The SBT consists of three ungrouped iron meteorites, Babb's Mill (Troost's Iron, herein referred to as Babb's Mill), South Byron, and Inland Forts 83500 (ILD 83500), which were recognized as having similar Ni, Ga, and Ge concentrations (17.5–17.8 wt. %, 18.6–20.0 ppm, 41.0–47.9 ppm, respectively) and ataxitic structures by Wasson et al. (1989). In addition to potentially originating from the same parent body, the SBT have been suggested to also be related to the ungrouped Milton pallasite. Several prior studies have noted chemical and isotopic

similarities between the SBT and the Milton pallasite, warranting study of this potential iron meteorite-pallasite relationship (Jones et al., 2003; McCoy et al., 2017).

In this study, the mass independent isotope systematics of some siderophile elements and the modeling of HSE, and Hf-W chronometry are employed to assess the nature of the possible relationship among the SBT meteorites, as well as to assess the HSE, S, P, and C contents of the parental melt. The short-lived Hf-W system ($^{182}Hf \rightarrow {}^{182}W + 2\beta^-$, $T_{1/2}$ = 8.9 Ma; Vockenhuber et al., 2004) is used to constrain the thermal history of the parent body including the timing of primary differentiation. Further, the potential relationship of the Milton pallasite to the SBT is evaluated using Mo and Ru isotopic compositions and chemical modeling.

2. Materials and Methods

2.1. Sample preparation

Samples of Milton and South Byron were obtained from the Smithsonian Institution, Department of Mineral Sciences, National Museum of Natural History. Babb's Mill was obtained from Arizona State University and ILD 83500 was obtained from the US Antarctic Meteorite Program. Pieces were cut from each meteorite sample using a water-cooled *Leco Vari-cut* saw and a 12.7 cm diamond-wafering blade. The blade was cleaned with carborundum prior to cutting each meteorite. Prior to dissolution, the surface of each cut meteorite piece was polished using a range of coarse- to fine-grit sandpaper to remove sawblade marks, and then sonicated multiple times in ethanol.

2.2. Isotopic measurements

Approximately 1–2 g pieces of each of the SBT irons and a 6 g piece of the Milton pallasite were dissolved in 40–120 mL 8M HCl at 130 °C for 72 hours in Teflon® beakers. The resulting solution was then centrifuged and the supernatant was divided into four aliquots to be separately processed for Os, Mo, Ru, and W isotopic measurements. Due to limited material, Milton was not processed for W. Details regarding the chemical and mass spectrometric procedures have been previously published (Worsham et al., 2016; Bermingham et al., 2016; Archer et al., 2017), reviewed in the supplementary materials, and briefly described here. Aliquots for Os isotopic analysis were oxidized in sealed Pyrex® Carius tubes with 2:1 HNO_3:HCl at 220 °C and then Os was extracted from the solution using CCl_4 solvent-extraction methods, and further purified using microdistillation techniques (Shirey and Walker, 1995; Cohen and Waters, 1996; Birck et al., 1997). Molybdenum aliquots were processed through three anion columns (Worsham et al., 2016) and Ru aliquots were processed through a cation column and then further purified using microdistillation techniques (Bermingham et al., 2016). Iron was removed from the W aliquots using a diisopropyl ether extraction procedure and then the aliquots were processed through a cation column and three anion columns (Dodson et al., 1936; Touboul and Walker, 2012). Isotopic compositions for Os, Mo, Ru, and W were measured by thermal ionization mass spectrometry (TIMS) at the University of Maryland (UMd).

The typical blanks for these procedures were <10 pg Os, <1 ng Mo, <10 pg Ru, and <1 ng W, which were inconsequential for the measurements reported here. Analytical uncertainty was assessed by measuring standard solutions multiple times (n>6) during an analytical campaign and assigning the two-standard deviation (2SD) value for the standards, which were always greater than the two-standard error (2SE) of the sample analyses, to the sample value. Reproducibility per analytical campaign of the Johnson Matthey Os standard (2SD) ranged from $^{189}Os/^{188}Os$ = 5–8 ppm and $^{190}Os/^{188}Os$ = 4–18 ppm, and the *Alfa Aesar Specpure®* Ru standard (2SD) was $^{100}Ru/^{101}Ru$ = 9–12 ppm. The reproducibility of the *Alfa Aesar Specpure®* W standard (2SD) was $^{182}W/^{184}W$ (186/184 normalized) = 6 ppm, $^{183}W/^{184}W$ = 6–7 ppm, and the *Alfa Aesar Specpure®* Mo standard (2SD) was $^{94}Mo/^{96}Mo$ = 10–26 ppm, $^{95}Mo/^{96}Mo$ = 8–15 ppm, and $^{97}Mo/^{96}Mo$ = 5–6 ppm. Results of isotopic measurements are reported in μ units (Eq. 1; e.g., Os).

$$\mu^{189}\mathrm{Os} = \left(\frac{\frac{189}{188}\mathrm{Os}_{\mathrm{sample}}}{\frac{189}{188}\mathrm{Os}_{\mathrm{standard}}} - 1 \right) * 1,000,000 \qquad \text{Eq. 1}$$

2.3. Isotope dilution

Concentration data for Re, Os, Ir, Ru, Pt, and Pd were obtained by isotope dilution using a chemistry procedure outlined in Walker et al. (2008). About 10–150 mg metal pieces of each meteorite were digested with 5 ml of concentrated HNO_3 and 2.5 ml of concentrated HCl, and equilibrated with a combined platinum-group element spike (^{191}Ir, ^{99}Ru, ^{194}Pt, and ^{105}Pd) and a Re-Os spike (^{185}Re and ^{190}Os) for at least 24 h at 220 °C in Pyrex® Carius tubes (Shirey and Walker, 1995). Once the tubes were opened, Os was separated and purified using the same techniques as discussed in the supplementary materials for unspiked Os samples. Spiked Os samples were separately analyzed by TIMS to determine Os concentrations and $^{187}Os/^{188}Os$ ratios (Cook et al., 2004). The remaining HSE were purified using an anion column procedure, an additional anion column was used for Re and Ru purification (Walker et al., 2008), and solutions were measured using a *Nu Plasma* multi-collector inductively-coupled plasma mass spectrometer at UMd. The blanks for these methods were typically <1 pg for Re and Os, and <30 pg for Ir, Ru, Pt, and Pd. Blank corrections were made but were not significant. The uncertainties for $^{187}Re/^{188}Os$ ratios were estimated to be ±0.15 %, the uncertainties for $^{187}Os/^{188}Os$, and Os and Re concentrations were estimated to be ±0.1 %, and the uncertainties for Ir, Ru, Pt, and Pd concentrations were estimated to be <2 % based on the reproducibility of similar samples using identical methods (Walker et al., 2008; McCoy et al., 2011).

3. Results

3.1. Osmium, Mo, Ru, and W isotopic results

Cosmic ray exposure (CRE) can result in neutron capture reactions within meteorites (Leya and Masarik, 2013). Such reactions can alter the Mo, Ru, and W isotopic compositions of a meteorite (e.g., Wittig et al., 2013; Worsham et al., 2017; Bermingham et al., 2018). The effects of CRE are dependent on the neutron fluence, which reflects both exposure duration

and depth from surface (e.g., Wittig et al., 2013). Consequently, CRE must be monitored and corrected for in the same meteorite piece as measured for mass independent and radiogenic isotopic compositions. Both Os and Pt isotopes have been applied to monitor and correct for CRE effects on siderophile elements (e.g., Walker et al., 2012; Kruijer et al., 2013; Wittig et al., 2013). Osmium is used as the dosimeter here, of which the $^{189}Os/^{188}Os$ ratio is most sensitive for assessing CRE effects. Increasingly greater CRE effects result in increasingly negative $\mu^{189}Os$ values. Based on the 2SD reproducibility (± 6–8 ppm) of the $^{189}Os/^{188}Os$ ratio of the terrestrial laboratory standard analyzed for this study, it is assumed that meteorite pieces with $\mu^{189}Os$ values within ± 8 ppm of zero were minimally affected by CRE. Milton, Babb's Mill, South Byron, and ILD 83500 have $\mu^{189}Os$ values ranging from −4 ± 8 to +8 ± 7, which are not resolved from the terrestrial standard (0 ± 8) (Table S1) and indicate that these meteorites were minimally affected by CRE. Of these four meteorites, Milton has the most negative $\mu^{189}Os$ value of −4 ± 8. Assuming a maximum expansion of error to a $\mu^{189}Os$ value of −12 ppm would require a CRE correction for $\mu^{97}Mo$ and $\mu^{100}Ru$ values of only −2 and +5 ppm, respectively, which are smaller than the measurement uncertainties of $\mu^{97}Mo$ and $\mu^{100}Ru$ values (Worsham et al., 2017; Bermingham et al., 2018). Of the meteorites measured for $\mu^{182}W$, Babb's Mill has the most negative $\mu^{189}Os$ value of +1 ± 6. In this case, the maximum expansion of error to a $\mu^{189}Os$ value of −5 ppm would require a CRE correction for $\mu^{182}W$ of −7 ppm, which is only slightly greater than the measurement uncertainty of $\mu^{182}W$ values to ±6 ppm (Worsham et al., 2017). Therefore, no CRE corrections have been made to the Mo, Ru, and W isotopic results for these meteorites.

The Mo and Ru isotopic compositions of Milton, Babb's Mill, South Byron, and ILD 83500 are provided in Table 1. These meteorites are characterized by a limited range of $\mu^{94}Mo$ values from +121 ± 13 to +132 ± 9, $\mu^{95}Mo$ values from +99 ± 9 to +104 ± 9, and $\mu^{97}Mo$ values from +46 ± 3 to +54 ± 5. Ruthenium isotopic compositions range from $\mu^{100}Ru$ = −104 ± 10 to −114 ± 15. Tungsten isotopic compositions are reported in Table 2. The measured $\mu^{182}W$ values for the SBT range from −307 ± 6 to −319 ± 6, and the measured $\mu^{183}W$ values range from +4 ± 7 to +15 ± 6. Collectively, the Mo and Ru isotopic compositions of the SBT and Milton, and the W isotopic compositions of the SBT are all identical, within analytical uncertainties.

3.2. ^{187}Re-^{187}Os and highly siderophile element concentrations

The ^{187}Re-^{187}Os chronometer is a useful tool for broadly constraining the age of metal crystallization, as well as evaluating open-system behavior of HSE. Osmium-187 is the β-decay product of ^{187}Re, which has a half-life of 41.6 Gyr (Smoliar et al., 1996). The ^{187}Re-^{187}Os results are reported in Table 3. The ^{187}Re-^{187}Os data were regressed using ISOPLOT (Ludwig, 2003) and the isochron yields an age of 4587 ± 230 Ma and an initial $^{187}Os/^{188}Os$ of 0.0953 ± 0.0019 (MSWD = 6.4). The limited range in Re/Os coupled with the limited number of meteorites result in the large uncertainty for these values, compared to some other groups (e.g., McCoy et al., 2011). Milton and the SBT all plot on or near a chondritic 4.568 Ga reference isochron (Fig. 2). These meteorites have Δ_{Os} values, calculated as the part per 10,000 deviation from the $^{187}Os/^{188}Os$ ratio of a sample to the reference isochron, ranging from −0.1 ± 2 to +3.9 ± 2. These results are consistent with

these meteorites experiencing limited open-system behavior for the HSE since crystallization in the early Solar System.

The HSE abundances of Milton metal and the SBT are reported in Table 3. Of the suite, Milton has the highest concentrations of Re, Os, Ir, Ru, and Pt, and the lowest concentration of Pd. The concentrations of HSE in Babb's Mill and South Byron are similar, with Babb's Mill slightly enriched in all of the HSE, except for Pd, compared to South Byron. ILD 83500 has the lowest concentrations of Re (approximately 10x less than Milton metal), Os, Ir, Ru, and Pt, and the highest concentration of Pd. The concentrations of Re and Ir in ILD 83500 are within 2 % of the concentrations reported by Wasson et al. (1989) and the Ir concentrations for Babb's Mill and South Byron are within 15 % of the concentrations reported by Scott et al. (1973). The concentrations of Re, Ir, and Pt reported by Jones et al. (2003) for Milton metal are within 20 % of the concentrations reported here.

4. Discussion

4.1. Genetics

Differences in the proportions of the nucleosynthetic components incorporated into NC and CC bodies allow for "genetic" comparisons of meteorites. For example, NC type meteorites have Mo and Ru isotopic compositions that reflect a constant *r*-process input with variable *s*-process depletion (Fig. 3, S1). Variations in $^{97}Mo/^{96}Mo$ and $^{100}Ru/^{101}Ru$ define a linear trend (Dauphas et al., 2004; Fischer-Gödde et al., 2015; Bermingham et al., 2018). By contrast, CC type meteorites have Mo and Ru isotopic compositions that reflect an additional *s*-process depletion (Fig. S1), and Mo and W isotopic compositions that reflect an additional *r*-process component (Fig. S2) (Kruijer et al., 2017).

The observation that the SBT have Mo, Ru, and ^{183}W isotopic compositions that are analytically indistinguishable provides permissive evidence that these meteorites sample the same parent body. If so, the isotopic data for the three meteorites can be averaged to obtain a more robust constraint on the isotopic characteristics of the parent body. The average $\mu^{94}Mo$, $\mu^{95}Mo$, and $\mu^{97}Mo$ values of the SBT meteorites are +127 ± 7, +103 ± 4, and +49 ± 2, respectively, where the uncertainties cited are 2SE. Further, the average $\mu^{100}Ru$ value is −107 ± 5 and the average $\mu^{183}W$ value is +9 ± 5. The average Mo and ^{183}W isotopic compositions of the SBT are identical, within analytical uncertainty, to those determined for the CC type IID, IIF, IIIF, and IVB iron meteorite groups (Fig. 3, S1, S2) (Budde et al., 2016; Kruijer et al., 2017; Poole et al., 2017; Worsham et al., 2017; Bermingham et al., 2018), and the average Ru isotopic composition of the SBT is identical to the CC type IID and IVB iron meteorite groups (Fischer-Gödde et al., 2015; Bermingham et al., 2018). Ruthenium isotopic data have not yet been determined for IIF and IIIF irons. Collectively, the genetic isotopic data indicate that the SBT should be defined as CC type meteorites. Because of the limited isotopic variation among CC irons, however, these isotopic systems are not useful for discriminating the SBT from most other known CC parent bodies.

The Mo and Ru isotopic compositions of Milton are indistinguishable from the SBT, providing permissive evidence for an origin on the SBT parent body, consistent with the identical O isotopic composition reported by McCoy et al. (2017). Thus, the Milton pallasite

should also be defined as a CC type meteorite, and it can be presumed that, at the very least, Milton and the SBT were derived from similar presolar materials, likely forming in the same region of the Solar nebula.

4.2. Crystallization sequence modeling of the SBT

Given the identical Mo, Ru, and ^{183}W isotopic compositions of the SBT to other CC type iron meteorite groups, it is imperative to test the possible SBT relationship through chemical modeling. The change in HSE concentrations among the SBT iron meteorites are broadly consistent with fractional crystallization in that the concentrations of Re, Os, Ir, Ru, and Pt typically decrease in crystallizing metal as the concentration of Pd increases. This trend is in agreement with the observation by Wasson et al. (1989) that, given the changes in As, Au, W, and Ir concentrations among these irons, the SBT could have originated by fractional crystallization. The similar HSE concentrations determined here for Babb's Mill and South Byron suggest that these irons crystallized at a similar point in a crystallization sequence. By contrast, ILD 83500 has about 17 % of the Re content and 130 % of the Pd content of Babb's Mill, indicating that, if they are related, ILD 83500 crystallized from a more evolved melt.

To examine further possible relationships resulting from fractional crystallization, we model HSE data for the SBT. To do this, appropriate solid metal-liquid metal D values (concentration ratios) must be applied. Some prior studies have derived relative D values for HSE for specific iron groups from the slopes of inter-element log-log plots (e.g., Campbell and Humayun, 2005; Walker et al., 2008; McCoy et al., 2011), coupled with experimental partitioning data for P or Ir, in order to model a crystallization sequence. However, due to the similar HSE concentrations of Babb's Mill and South Byron, the data for the SBT essentially define two-point lines. For this reason, we use the approach developed by Jones and Malvin (1990) and advanced by Chabot and Jones (2003) and Chabot et al. (2017), which uses experimentally derived partitioning data for siderophile elements in the Fe-Ni-S, Fe-Ni-P, and Fe-Ni-C systems to determine the D values for HSE for given S, P, and C contents. A more detailed description of this approach is provided in the supplementary materials.

Here we constrain the initial P content of the SBT parental melt by coupling the measured P content of Babb's Mill and South Byron (0.12–0.22 wt. % P) reported in Buchwald (1975) with a solid metal-liquid metal partition coefficient of 0.1 (Chabot et al., 2017). This suggests a P content in the melt of about 1 wt. % at the point where these two irons crystallized. The initial S content was then varied along with different HSE initial melt compositions until a model crystallization sequence was generated that matched the SBT HSE concentrations.

The optimal initial light-element concentrations determined are 7 wt. % S, 1 wt. % P, and <0.05 wt. % C. This model reproduces the HSE abundances of the SBT through fractional crystallization of an initial parental melt with chondritic relative abundances of the HSE. The model matches the HSE concentration of Babb's Mill as the first 1 % of metal to crystallize. South Byron is reproduced as 2 % of metal to crystallize, and ILD 83500 matches the solid HSE composition at 42 % crystallization (Fig. 4).

The calculated initial parental melt HSE composition for the SBT (Table 4) is shown in Fig. 5, normalized to the CI-chondrite Orgueil (Horan et al., 2003; Fischer-Gödde et al., 2010). This initial melt composition has Re/Os, Ir/Os, Ru/Os, Pt/Os, and Pd/Os ratios of 0.082, 0.90, 1.1, 1.7, and 0.89, respectively, which are all within the ranges of ratios observed in bulk chondrites of 0.059–0.101, 0.77–1.02, 1.1–2.0, 1.4–2.5, and 0.54–2.01, respectively (Horan et al., 2003; Fischer-Gödde et al., 2010).

The calculated initial parental melt HSE composition of the SBT is about 10 times more concentrated than the upper range of HSE concentrations in chondrites. If this upper range is assumed to represent the starting concentration of the SBT parent body, and if it is assumed that ~99 % of the HSE were extracted into the core, then the SBT parental melt would have accounted for ~10 % the mass of the body. This result suggests that the SBT represent samples of a planetesimal core and should be considered magmatic iron meteorites. Past studies have estimated the parental melt compositions for the magmatic IVA and IVB iron meteorites (Walker et al., 2008; McCoy et al., 2011). The modeled HSE parental melt composition of the SBT parent body falls between the compositions previously estimated for the parent bodies of the group IVA and IVB iron meteorites (Fig. 5). As suggested for the IVB parent body, the high HSE concentration of the SBT parental melt may suggest a comparatively oxidized body. In this scenario, a greater proportion of oxidized iron would remain in the mantle compared to a more reduced body, resulting in relatively higher concentrations of HSE in the core. An oxidized SBT body is also supported by the high Ni content (17–18 wt. %) of these meteorites.

4.3. Crystallization sequence modeling of Milton

Since Mo, Ru, and O isotopic compositions of Milton and the SBT only provide permissive evidence of a common parent body, a potential relationship for these meteorites is further evaluated through chemical modeling. Milton metal has a Pt/Os ratio that is similar to that for Babb's Mill, which is estimated to represent the first 1 % of metal to crystallize, yet a Re/Os ratio that is similar to ILD 83500, which is estimated to represent crystallization at 42 %. Attempts were made to model Milton as part of the same solid metal-liquid metal fractional crystallization sequence as the SBT by varying the initial HSE, S, P, and C contents of the system. Changes to the initial S, P, or C contents can have large effects on the concentration of HSE in crystallizing metal, however, such changes cannot account for the Re/Os and Pt/Os ratios observed for Milton. An example of the modeling is shown in Fig. S3.

Modeling involving solid metal-liquid metal mixing was also undertaken in an attempt to relate Milton metal to the SBT. Metal mixing of primitive and evolved metals from the core along with residual metal in the mantle has been suggested for the formation of the main group pallasites on the IIIAB iron meteorite parent body (Scott, 1977b; Wasson and Choi, 2003). Such models failed to reproduce Re/Os and Pt/Os ratios for Milton and were, therefore, unsuccessful at relating Milton metal and the SBT to the same metal system (Fig. S4). Consideration was also given to the crystallization of Milton metal and the SBT from two immiscible metal melts (one P rich and one S rich) within the same core. Models of metal liquid immiscibility have been invoked for the IID iron meteorites (Wasson and Huber,

2006) and to relate the IIAB irons to the IIG irons (Wasson and Choe, 2009). Milton metal has a similar P content to Babb's Mill and South Byron, however, which suggests that they did not form from immiscible metal melts (McCoy et al., 2017). Due to the lack of models that can reproduce the SBT and Milton metal HSE concentrations from the same metal liquid, we conclude that Milton metal was most likely not generated from the parental melt to the SBT.

The HSE concentrations in Milton metal suggest a parental melt that was characterized by several HSE ratios outside of the range observed in known bulk chondrites. Examples of three possible parental melt compositions, which can reproduce Milton metal as an early fractional crystallizing metal, are shown in Fig. S5. For these three models, we assume parental melt abundances of 1 wt. % S, 1 wt. % P, <0.05 wt. % C; 5 wt. % S, 2 wt. % P, <0.05 wt. % C; and 10 wt. % S, 3 wt. % P, <0.05 wt. % C. All three models are characterized by calculated parental melt Re/Os ratios (0.12, 0.13 0.15) and Ir/Os ratios (1.05, 1.04, 1.10) that are 2 to 50% above the range observed in bulk chondrites (Horan et al., 2003; Fischer-Gödde et al., 2010). By contrast, all Pt/Os ratios (1.4, 1.5, 1.8), and most Ru/Os ratios (1.1, 1.5, 2.5) and Pd/Os ratios (0.43, 0.73, 1.88) are within the range of bulk chondrites.

It is possible that such parental melts described above existed on the SBT parent body without interacting with the SBT parental melt, or may have been generated through the mixing of variable amounts of liquid metal or solid metal from the SBT crystallization sequence with a metal source with fractionated relative abundances of some HSE compared to bulk chondrites. Generating and maintaining these separate metal domains within the same planetesimal, however, is difficult to envision. Hence, it is more likely that Milton formed on a chemically distinct, but genetically identical parent body to the SBT. This interpretation would expand the number of chemically distinct parent bodies with identical Mo, Ru, and O genetic isotopic compositions to at least three (e.g., SBT, Milton, and IVB irons; Corrigan et al., 2017; McCoy et al., 2017; Bermingham et al., 2018).

As may be the case for Milton, the parental melt to the IVB iron meteorites was likely non-chondritic with respect to the relative abundances of some HSE (Campbell and Humayun, 2005; Walker et al., 2008). Campbell and Humayun (2005) and Walker et al. (2008) suggested that the volatile siderophile element depletions projected for the IVB parent body may have resulted from high temperature condensation processes. Such a model is less plausible for the Milton parent body, as the meteorite is significantly enriched in volatile siderophile elements, such as Ga and Ge, compared to the IVB irons (Walker et al., 2008; McCoy et al., 2017). The three parental melt compositions for Milton modeled in this study are characterized by Re/Os and Ir/Os ratios that are suprachondritic. Both Re/Os and Ir/Os tend to increase as a consequence of crystal liquid fractionation (see above modeling of SBT) so it is possible that the parental melt to Milton represents a modestly evolved liquid that was somehow segregated from earlier formed solids. This could potentially have occurred on the parent body as a result of hit and run impacts followed by core dismemberment, melting, and recrystallization, as suggested for the group IVA iron meteorites in order to explain rapid rates of cooling in the least evolved members (McCoy et al., 2011).

4.4. Age of the SBT

The identical Mo, Ru, and ^{183}W isotopic compositions of the SBT and the ability to relate the HSE concentrations of these meteorites through crystal-liquid fractionation provide permissive evidence that the SBT meteorites originated on the same parent body and are related by fractional crystallization from a common melt. The average μ^{182}W value for this body is −312 ± 5 and the average μ^{183}W value is +9 ± 5. As has been done for other CC type iron meteorites (e.g., Kruijer et al., 2017), the μ^{182}W value is corrected for additional *r*-process input revealed by the ^{183}W excess, yielding an average $\mu^{182}W_{Corr}$ value of −325 ± 8 (see supplementary materials for details). The $\mu^{182}W_{Corr}$ value of the SBT is not resolved from the $\mu^{182}W_{Corr}$ values of other CC type iron meteorites or NC type iron meteorites, except the IC and IIAB groups (Kruijer et al., 2017). The $\mu^{182}W_{Corr}$ value of the SBT parent body results in a ^{182}W model age of 2.1 ± 0.8 Myr after calcium aluminum rich inclusion (CAI) (Fig. 6), which is not resolved from other CC type or NC type iron meteorite parent bodies, except for the IC and IIAB groups (Kruijer et al., 2017). This differentiation age is within the lifetime of ^{26}Al, allowing for the differentiation event to have been driven by internal heating, consistent with the interpretation that the SBT are magmatic iron meteorites formed in the core of the SBT parent body.

Differentiation ages can be used to estimate parent body accretion ages by making certain assumptions regarding the time required for a parent body to heat sufficiently to allow metal-silicate segregation. Based on this reasoning, Kruijer et al. (2017) proposed that all NC type iron meteorite parent bodies accreted simultaneously about 0.5 Myr prior to the accretion of all CC type iron meteorite parent bodies. This conclusion relied on the averaging of data for only Groups I and II (volatile rich) irons. To estimate a separate parent body accretion age for the SBT, we use a similar thermal model to that described by Kruijer et al. (2017), which calculates the heat produced from ^{26}Al, the primary heat producing radionuclide during the early Solar System. Details about this model are provided in the supplementary materials. Uncertainties for the model accretion ages represent the range of accretion ages calculated using the range of Al concentrations and differentiation age uncertainties. For the SBT parent body, the differentiation age, coupled with an assumed Al concentration range of 0.86–1.68 wt. % for the parent body, based on the range of Al concentrations found in carbonaceous chondrites (Lodders and Fegley, 1998), corresponds to a parent body accretion age of 1.1 ± 0.5 Myr after CAI formation (Fig. S6). Because of differences in the calculation of heat production, our thermal model differs somewhat from that of Kruijer et al. (2017). To facilitate comparisons, accretion ages for other iron meteorite parent bodies were recalculated using our model coupled with the differentiation ages reported by Kruijer et al. (2017) (Table 5). When considering the uncertainties associated with ^{182}W differentiation ages, NC type iron meteorite parent bodies have accretion ages ranging from 0.3 ± 0.3 to 1.0 ± 0.5 Myr after CAI formation, whereas CC type iron meteorite parent bodies have accretion ages from 1.1 ± 0.5 to 1.4 ± 0.5 Myr after CAI formation. Uncertainties of ~0.5 Myr for each body mean that permissible model ages of accretion for both CC and NC types overlap.

Kruijer et al. (2017) argued that the assumptions behind a single-stage core formation accretion model at a certain temperature are affected by the volatile-enrichment or depletion of the parent body, so it is important to compare iron meteorite parent bodies from the same

volatile type. Kruijer et al. (2017) found that the CC type IIC, IID, and IIF irons have $\mu^{182}W_{Corr}$ values that are resolved from the NC type IIAB irons, which was argued to suggest that CC type iron meteorite parent bodies accreted later than NC type iron meteorite parent bodies. The accretion age results of our preferred thermal model, however, overlap for the NC type IIAB and the CC type IIC, IID, and IIF irons. In addition, the NC type IIIAB and IIIE irons have accretion ages that overlap with the CC type IIIF and SBT accretion ages. There is also overlap among the NC type IVA and the CC type IVB accretion ages. Thus, we conclude that NC and CC type iron meteorite parent body accretion ages cannot be resolved at present, given the current level of uncertainties associated with parent body differentiation ages and Al content.

Since differences in accretion ages cannot explain the differences in $\mu^{182}W_{Corr}$ values for Group II irons with current uncertainties, we examine the effects of S content on differentiation. Kruijer et al. (2014b) showed that there was a correlation between S content of a parental melt with $\mu^{182}W_{Corr}$ values for the IIAB, IIIAB, IVA, IID, and IVB irons. The determination of the S content for the SBT parent body allows for a reexamination of this correlation with three NC and three CC bodies. The S *vs.* $\mu^{182}W_{Corr}$ value of the SBT falls directly on the correlation and reduces the scatter observed for the IID and IVA iron meteorites (Fig. 7). The six meteorites define a single trend with a MSWD = 2.7, which may suggest that the S content of a parental melt is the controlling factor for $\mu^{182}W_{Corr}$ values, possibly by affecting the temperature at which metal melting and differentiation begins. Further studies to define the S content of other NC and CC type iron parental melts are needed to evaluate this potential correlation.

4.5. Comparison of the SBT chemical composition to NC and CC bodies

The HSE parental melt models of the CC type SBT and IVB iron meteorites, and the NC type IVA iron meteorites provide new insights into the chemical conditions of the NC and CC nebular domains. The SBT and IVB iron meteorites have parental melt HSE compositions that are 2–7 times more concentrated than the IVA parent body. Presuming that the concentrations are directly related to the ratio of core metal to silicate shell, this result suggests that the SBT and IVB iron meteorite parent bodies had proportionally smaller cores than NC type parent bodies, and therefore most likely accreted in more oxidizing environments, compared to, e.g., the IVA parent body. Previous studies have proposed that the NC and CC domains represent the inner and outer Solar System, respectively, that were separated by the formation of Jupiter (Warren, 2011; Budde et al., 2016; Kruijer et al., 2017). Such a model could account for the more oxidizing environment of the SBT and IVB parent bodies.

Additional chemical differences are observed for NC and CC parental melts when comparing S content. Past studies, also using experimentally derived partitioning data for siderophile elements in the Fe-Ni-S, Fe-Ni-P, and Fe-Ni-C systems to determine D values, have concluded that the IIAB, IIIAB, IVA, IID, and IVB iron meteorite parental melts had S contents of 17 ± 1.5, 12 ± 1.5, 6 ± 3, 9 ± 3, and 1 ± 1 wt. %, respectively (Chabot, 2004; Goldstein et al., 2009). When iron meteorites are compared based on volatile content, there is an additional S depletion for CC parental melts compared to NC parental melts (Fig. 8).

This additional depletion in S may reflect parent body processes more common on CC type parent bodies, such as core separation into S-rich and P-rich liquids, or may be a consequence of nebular processes.

5. Conclusions

The isotopic and chemical data presented here for Babb's Mill, South Byron, and ILD 83500 support the interpretation that these meteorites sample a core from the same parent body and that they should be considered together as a trio.

1. The SBT parent body originated in the CC nebular domain, based on Mo, Ru, and ^{183}W isotopic data. Thermal modeling indicates the parent body likely accreted 1.1 ± 0.5 Myr after CAI formation and the Hf-W isotopic system indicates that the parent body differentiated 2.1 ± 0.8 Myr after CAI formation. Both accretion and differentiation ages are similar to the ages for other NC and CC type iron meteorite parent bodies.

2. The siderophile element concentrations of the SBT suggest that Babb's Mill crystallized from a primitive melt, followed soon afterward by South Byron. ILD 83500 crystallized later in the sequence from a more evolved melt. The HSE patterns of these meteorites can be reproduced by a fractional crystallization model, in which Babb's Mill represents the first 1 % of solid to crystallize. South Byron can be modeled as the solid composition after 2 % crystallization, and ILD 83500 represents the solid composition at 42 % crystallization. This model suggests an initial melt composition of 7 wt. % S, 1 wt. % P, <0.05 wt. % C, and a HSE initial melt composition with chondritic HSE ratios.

3. The bulk concentrations of the HSE in the SBT parental core suggest that it comprised about 10 % the mass of the body, assuming the upper range of HSE concentrations observed in chondrites as a starting parent body composition. This in turn suggests that the SBT parent body was oxidized, which is also consistent with the comparatively high average Ni content for the SBT (17–18 wt. % Ni).

4. Milton has identical Mo and Ru isotopic compositions to the SBT, providing permissive evidence of being from the same parent body. The HSE content of Milton, however, cannot be directly related to the SBT by fractional crystallization or any other process we attempted to model. Milton metal was likely derived from a parental melt with relative abundances of some HSE that were modestly fractionated from known chondritic ratios, most likely on a different parent body from the SBT.

5. Comparison of modeled HSE parental melt compositions of the SBT to the IVA (NC) and IVB (CC) iron meteorite parent bodies provides further evidence that portions of the CC nebular domain were more oxidizing than the NC domain. In addition, comparison of the S parental melt compositions of the IIAB, IIIAB, IVA, IID, SBT, and IVB iron meteorites suggest that there was a general S

depletion among CC type iron meteorite parental melts, compared to NC type bodies.

Supplementary Material

Refer to Web version on PubMed Central for supplementary material.

Acknowledgments

We gratefully acknowledge the Smithsonian Institution, Arizona State University, and the US Antarctic Meteorite Program, which is a cooperative venture of the Smithsonian, NASA and the National Science Foundation, for providing access to the samples for this study. We also thank Frederic Moynier, Thomas Kruijer, and two anonymous reviewers for helpful comments that improved the manuscript. This study was supported by NASA Emerging Worlds grant NNX16AN07G (to RJW).

References

Archer GJ, Mundl A, Walker RJ, Worsham EA, Bermingham KR (2017) High-precision analysis of $^{182}W/^{184}W$ and $^{183}W/^{184}W$ by negative thermal ionization mass spectrometry: per-integration oxide corrections using measured $^{18}O/^{16}O$. Int. J. Mass Spectrom 414, 80–86. [PubMed: 30713466]

Birck J-L, Roy-Barman M, Capmas F (1997) Re–Os isotopic measurements at the femtomole level in natural samples. Geostand. Newsl 20, 9–27.

Bermingham KR, Walker RJ, Worsham EA (2016) Refinement of high precision Ru isotope analysis using negative thermal ionization mass spectrometry. Int. J. Mass Spectrom 403, 15–26. [PubMed: 30713465]

Bermingham KR, Worsham EA, Walker RJ (2018) New insights into Mo and Ru isotope variation in the nebula and terrestrial planet accretionary genetics. Earth Planet. Sci. Lett 487, 221–229. [PubMed: 30880823]

Buchwald VF (1975) Handbook of Iron Meteorites. University of California Press, Berkeley, CA.

Budde G, Burkhardt C, Brennecka GA, Fischer-Godde M, Kruijer TS, Kleine T (2016) Molybdenum isotopic evidence for the origin of chondrules and a distinct heritage of carbonaceous and non-carbonaceous meteorites. Earth Planet. Sci. Lett 454, 293–303.

Burkhardt C, Kleine T, Oberli F, Pack A, Bourdon B, Wieler R (2011) Molybdenum isotope anomalies in meteorites: constraints on solar nebula evolution and origin of the Earth. Earth Planet. Sci. Lett 312, 390–400.

Campbell AJ and Humayun M (2005) Compositions of group IVB iron meteorites and their parent melt. Geochim. Cosmochim. Acta 69, 4733–4744.

Chabot NL (2004) Sulfur contents of the parental metallic cores of magmatic iron meteorites. Geochim. Cosmochim. Acta 68, 3607–3618.

Chabot NL and Jones JH (2003) Parameterizing iron meteorite partitioning experiments. Meteorit. Planet. Sci 37, 1425–1436.

Chabot NL, Wollack EA, McDonough WF, Ash RD, Saslow SA (2017) Experimental determination of partitioning in the Fe-Ni system for applications to modeling meteoritic metals. Meteorit. Planet. Sci 52, 1133–1145. [PubMed: 28943752]

Chen JH, Papanastassiou DA, Wasserburg GJ (2010) Ruthenium endemic isotope effects in chondrites and differentiated meteorites. Geochim. Cosmochim. Acta 74, 3851–3862.

Cohen AS and Waters FJ (1996) Separation of osmium from geological materials by solvent extraction for analysis by thermal ionization mass spectrometry. Anal. Chimica Acta 332, 269–275.

Cook DL, Walker RJ, Horan MF, Wasson JT, Morgan JW (2004) Pt–Re–Os systematics of group IIAB and IIIAB iron meteorites. Geochim. Cosmochim. Acta 68, 1413–1431.

Corrigan CM, McCoy TJ, Nagashima K (2017) Oxygen isotopes of chromite in IVB iron meteorites: relationships to other meteorite groups and implications for formation. Lunar Planet. Sci. Conf XLVIII, 2556 (abst).

Dauphas N, Marty B, Reisberg L (2002) Molybdenum evidence for inherited planetary scale isotope heterogeneity of the protosolar nebula. Astrophys. Journ 565, 640–644.

Dauphas N, Davis AM, Marty B, Reisberg L (2004) The cosmic molybdenum-ruthenium isotope correlation. Earth Planet. Sci. Lett 226, 465–475.

Dodson RW, Forney GJ, Swift EH (1936) The extraction of ferric chloride from hydrochloric acid solutions by isopropyl ether. J. Am. Chem. Soc 58, 2573–2577.

Fischer-Gödde M, Becker H, Wombacher F (2010) Rhodium, gold, and other highly siderophile element abundances in chondritic meteorites. Geochim. Cosmochim. Acta 74, 356–379.

Fischer-Gödde M, Burkhardt C, Kruijer TS, Kleine T (2015) Ru isotope heterogeneity in the solar protoplanetary disk. Geochim. Cosmochim. Acta 168, 151–171.

Goldstein JI, Scott ERD, Chabot NL (2009) Iron meteorites: Crystallization, thermal histories, parent bodies, and origin. Chemie der Erde 69, 293–325.

Horan MF, Walker RJ, Morgan JW, Grossman JN, Rubin AE (2003) Highly siderophile elements in chondrites. Chem. Geol 196, 5–20.

Jones JH and Malvin DJ (1990) A nonmetal interaction model for the segregation of the trace metals during solidification of Fe–Ni–S, Fe–Ni–P, Fe–Ni–S–P alloys. Metall. Trans. B 21B, 697–706.

Jones RH, Wasson JT, Larson T, Sharp ZD (2003) Milton: a new, unique pallasite. Lunar Planet. Sci. Conf XXXIV, 1683 (abst).

Kruijer TS, Fischer-Gödde M, Kleine T, Sprung P, Leya I, Wieler R (2013) Neutron capture on Pt isotopes in iron meteorites and the Hf-W chronology of core formation in planetesimals. Earth Planet. Sci. Lett 361, 162–172.

Kruijer TS, Kleine T, Fischer-Gödde M, Burkhardt C, Wieler R (2014a) Nucleosynthetic W isotope anomalies and the Hf-W chronometry of Ca-Al-rich inclusions. Earth Planet. Sci. Lett 403, 317–327.

Kruijer TS, Touboul M, Fischer-Gödde M, Bermingham KR, Walker RJ, Kleine T (2014b) Protracted core formation and rapid accretion of protoplanets. Science 344, 1150–1154. [PubMed: 24904163]

Kruijer TS, Burkhardt C, Budde G, Kleine T (2017) Age of Jupiter inferred from the distinct genetics and formation times of meteorites. Proc. Natl. Acad. Sci 114, 6712–6716. [PubMed: 28607079]

Leya I and Masarik J (2013) Thermal neutron capture effects in radioactive and stable nuclide systems. Meteorit. Planet. Sci 48, 665–685.

Lodders K and Fegley B (1998) The Planetary Scientist’s Companion. Oxford Univ Press, New York, 371 pp.

Ludwig KR (2003) User’s Manual for Isoplot 3.00. Berkeley Geochronology Center Special Publication No. 4, Berkeley, CA, 70 pp.

McCoy TJ, Walker RJ, Goldstein JI, Yang J, McDonough WF, Rumble D, Chabot NL, Ash RD, Corrigan CM, Michael JR, Kotula PG (2011) Group IVA irons: new constraints on the crystallization and cooling history of an asteroidal core with a complex history. Geochim. Cosmochim. Acta 75, 6821–6843.

McCoy TJ, Corrigan CM, Nagashima K, Reynolds VS, Walker RJ, McDonough WF, Ash RD (2017) Milton and the South Byron Trio: an oxidized parent body with an outside-in crystallization core. Lunar Planet. Sci. Conf XLVIII, 2241 (abst).

Poole GM, Rehkamper M, Coles BJ, Goldberg T, Smith CL (2017) Nucleosynthetic molybdenum isotope anomalies in iron meteorites-new evidence for thermal processing of solar nebula material. Earth Planet. Sci. Lett 473, 215–226.

Qin L, Dauphas N, Janney PE, Wadhwa M (2008) Tungsten nuclear anomalies in planetesimal cores. Astrophys. Journ 674, 1234–1241.

Schaudy R and Wasson JT (1972) The chemical classification of iron meteorites. VI. A reinvestigation of irons with Ge concentrations lower than 1 ppm. Icarus 17, 174–192.

Scott ERD, Wasson JT, Buchwald VF (1973) The chemical classification of iron meteorites-VII. A reinvestigation of irons with Ge concentrations between 25 and 80 ppm. Geochim. Cosmochim. Acta 37, 1957–1983.

Scott ERD and Wasson JT (1976) Chemical classification of iron meteorites-VIII. Groups IC, IIE, IIIF and 97 other irons. Geochim. Cosmochim. Acta 40, 103–115.

Scott ERD (1977a) Composition, mineralogy and origin of group IC iron meteorites. Earth Planet. Sci. Lett 37, 273–284.

Scott ERD (1977b) Geochemical relationships between some pallasites and iron meteorites. Mineralogical magazine 41, 265–272.

Shirey SB and Walker RJ (1995) Carius tube digestion for low-blank rhenium-osmium analysis. Anal. Chem 34, 2136–2141.

Shirey SB and Walker RJ (1998) The Re-Os isotope system in cosmochemistry and high-temperature geochemistry. Annu. Rev. Earth Planet. Sci 26, 423–500.

Smoliar MI, Walker RJ, Morgan JW (1996) Re–Os ages of group IIA, IIIA, IVA, and IVB iron meteorites. Science 271, 1099–1102.

Touboul M and Walker RJ (2012) High precision tungsten isotope measurement by thermal ionization mass spectrometry. Int. J. of Mass Spectrom 309, 109–117.

Vockenhuber C, Oberli F, Bichler M, Ahmad I, Quittem G, Meier M, Halliday AN, Lee DC, Kutschera W, Steier P, Gehrke RJ, Helmer RG (2004) New half-life measurement of ^{182}Hf: Improved chronometer for the early solar system. Physical Review Letters 93, 172501-1–172501-4. [PubMed: 15525068]

Walker RJ, McDonough WF, Honesto J, Chabot NL, McCoy TJ, Ash RD, Bellucci JJ (2008) Modeling fractional crystallization of group IVB iron meteorites. Geochim. Cosmochim. Acta 72, 2198–2216.

Walker RJ (2012) Evidence for homogeneous distribution of osmium in the protosolar nebula. Earth Planet. Sci. Lett 351–352, 36–44.

Warren PH (2011) Stable-isotopic anomalies and the accretionary assemblage of the Earth and Mars: a subordinate role for carbonaceous chondrites. Earth Planet. Sci. Lett 311, 93–100.

Wasson JT (1969) The chemical classification of iron meteorites-III. Hexadrites and other irons with germanium concentrations between 80 and 200 ppm. Geochim. Cosmochim. Acta 33, 859–876.

Wasson JT (1999) Trapped melt in IIIAB irons: solid/liquid elemental partitioning during the fractionation of the IIIAB magma. Geochim. Cosmochim. Acta 63, 2875–2889.

Wasson JT and Choe W-H (2009) The IIG iron meteorites: Probable formation in the IIAB core. Geochim. Cosmochim. Acta 73, 4879–4890.

Wasson JT and Choi B-G (2003) Main-group pallasites: chemical composition, relationship to IIIAB irons, and origin. Geochim. Cosmochim. Acta 67, 3079–3096.

Wasson JT and Huber H (2006) Compositional trends among IID irons; their possible formation from the P-rich lower magma in a two-layer core. Geochim. Cosmochim. Acta 70, 6153–6167.

Wasson JT, Huber H, Malvin DJ (2007) Formation of IIAB iron meteorites. Geochim. Cosmochim. Acta 71, 760–781.

Wasson JT, Ouyang X, Wang J, Jerde E (1989) Chemical classification of iron meteorites: XI. Multi-element studies of 38 new irons and the high abundance of ungrouped irons from Antarctica. Geochim. Cosmochim. Acta 53, 735–744.

Wasson JT and Richardson JW (2001) Fractional trends among IVA iron meteorites: contrasts with IIIAB trends. Geochim. Cosmochim. Acta 65, 951–970.

Wittig N, Humayun M, Brandon AD, Huang S, Leya I (2013) Coupled W-Os-Pt isotope systematics in IVB iron meteorites: In situ neutron dosimetry for W isotope chronology. Earth Planet. Sci. Lett 361, 152–161.

Worsham EA, Walker RJ, Bermingham KR (2016) High-precision molybdenum isotope analysis by negative thermal ionization mass spectrometry. Int. J. Mass Spectrom 407, 51–61. [PubMed: 30842700]

Worsham EA, Bermingham KR, Walker RJ (2017) Characterizing cosmochemical materials with genetic affinities to the Earth: Genetic and chronological diversity within the lAB iron meteorite complex. Earth Planet. Sci. Lett 467, 157–166. [PubMed: 30713346]

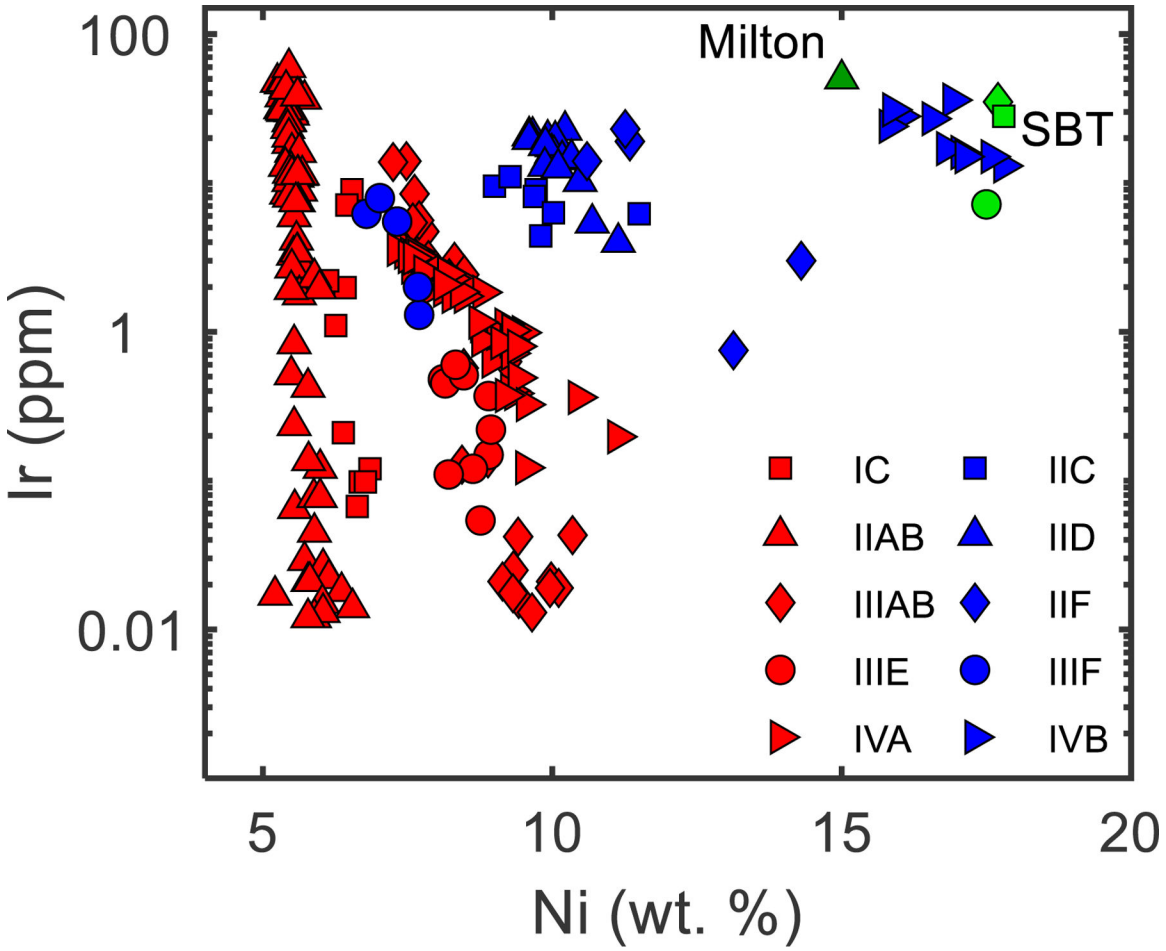

Fig. 1.

Compilation of Ni *vs.* Ir concentration data for the magmatic iron meteorite groups. Blue symbols represent CC type meteorites and red symbols represent NC type meteorites. Milton and the SBT are shown as dark and light green symbols, respectively. Data are compiled from Wasson (1969), Schaudy and Wasson (1972), Scott et al. (1973), Scott and Wasson (1976), Scott (1977a), Wasson et al. (1989), Wasson (1999), Wasson and Richardson (2001), Jones et al. (2003), Wasson and Huber (2006), and Wasson et al. (2007).

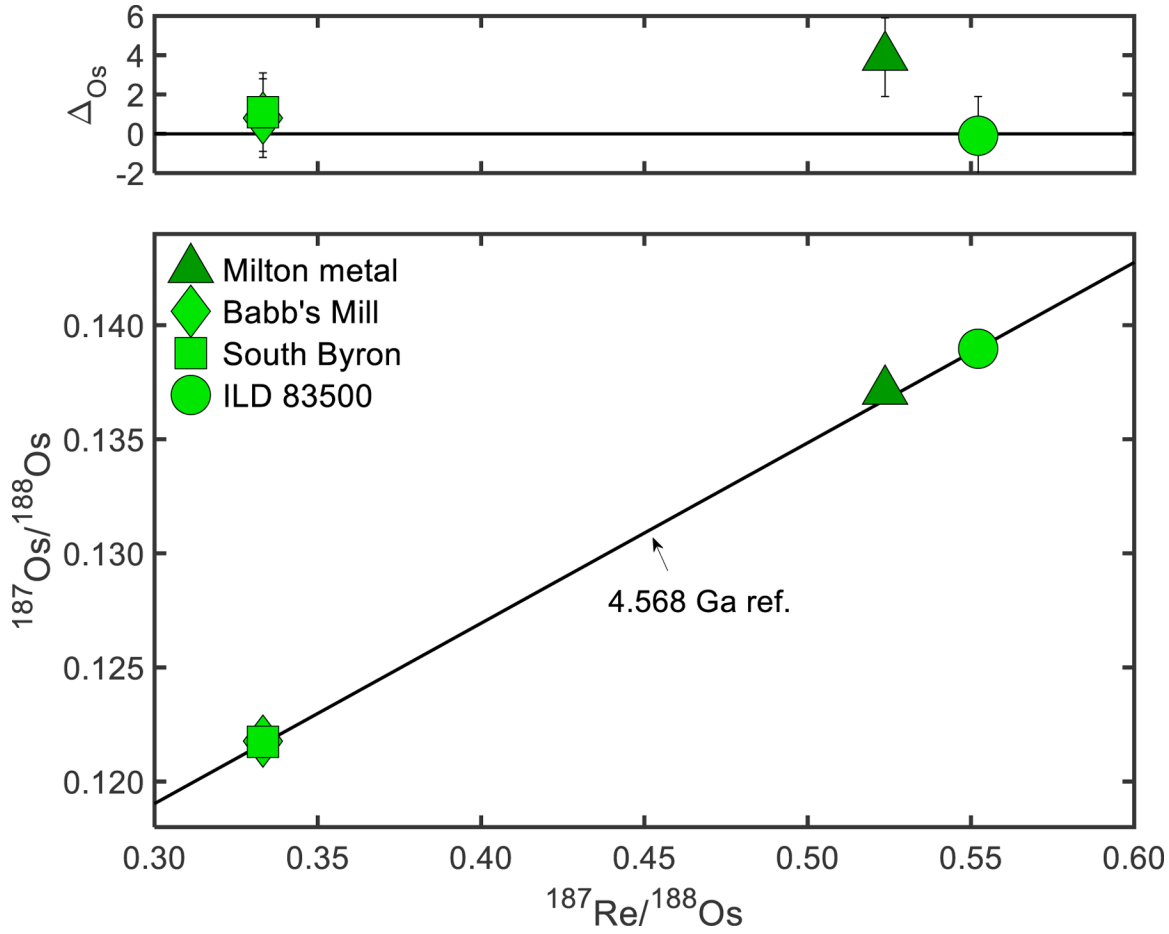

Fig. 2.

(Top) $^{187}Re/^{188}Os$ *vs.* Δ_{Os} plot for the Milton metal and SBT, where Δ_{Os} is the parts per 10,000 deviation of the $^{187}Os/^{188}Os$ ratio of a sample from a 4.568 Ga reference line. (Bottom) $^{187}Re/^{188}Os$ *vs.* $^{187}Os/^{188}Os$ plot for the Milton metal and SBT. Reference line represents the 4.568 Ga hypothetical evolution of the $^{187}Os/^{188}Os$ ratio in chondrites, assuming an initial $^{187}Os/^{188}Os = 0.09531$, present day chondritic $^{187}Os/^{188}Os = 0.1270$ and $^{187}Re/^{188}Os = 0.40186$, and $\lambda = 1.666 \times 10^{-11}$ yr^{-1} (Smoliar et al.,1996; Shirey and Walker, 1998).

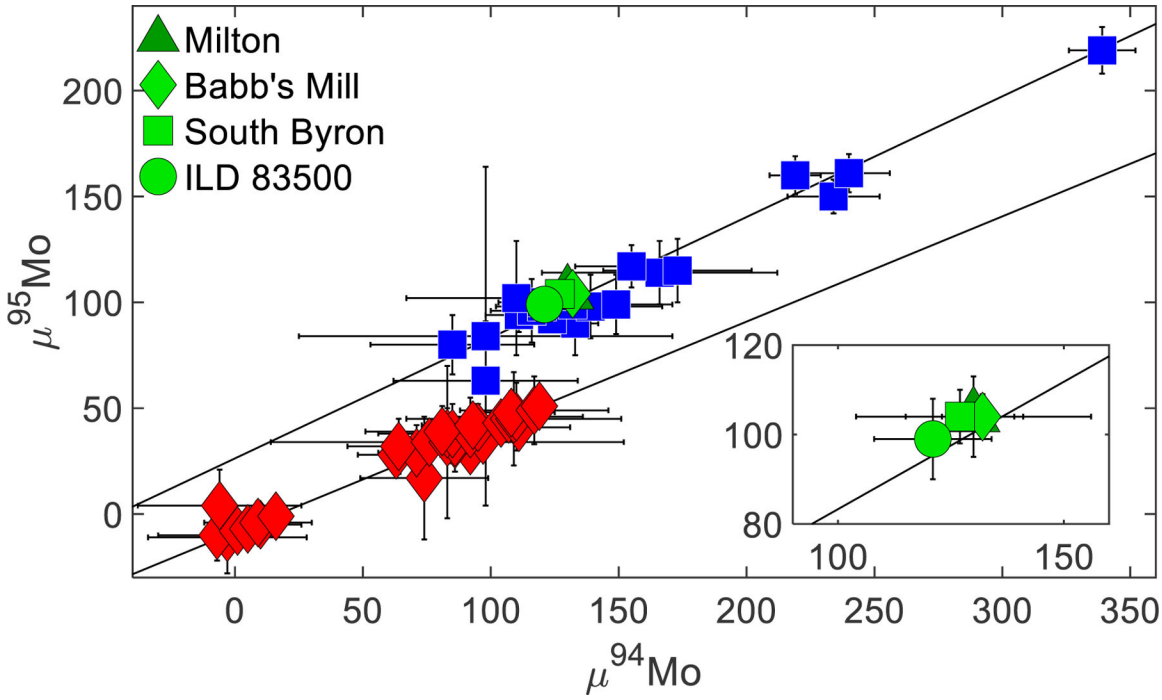

Fig. 3.

Compilation of μ^{94}Mo *vs.* μ^{95}Mo data for iron meteorites and pallasites from Burkhardt et al. (2011), Kruijer et al. (2017), Poole et al. (2017), and Worsham et al. (2017). Some data have not been corrected for CRE. Blue squares represent meteorites classified as CC type and red diamonds represent meteorites classified as NC type. Data from this study for the SBT and Milton are also plotted. Black lines were obtained by regressing the NC and CC data using ISOPLOT (Ludwig, 2003); the CC line has a slope of 0.57 ± 0.05 and a y-intercept of 26.3 ± 7.5 (MSWD = 1.15) and the NC line has a slope of 0.50 ± 0.04 and a y-intercept of −8.5 ± 3.2 (MSWD = 0.49). The inset shows an enlarged view of the Mo isotopic compositions of the SBT and Milton without other meteorites.

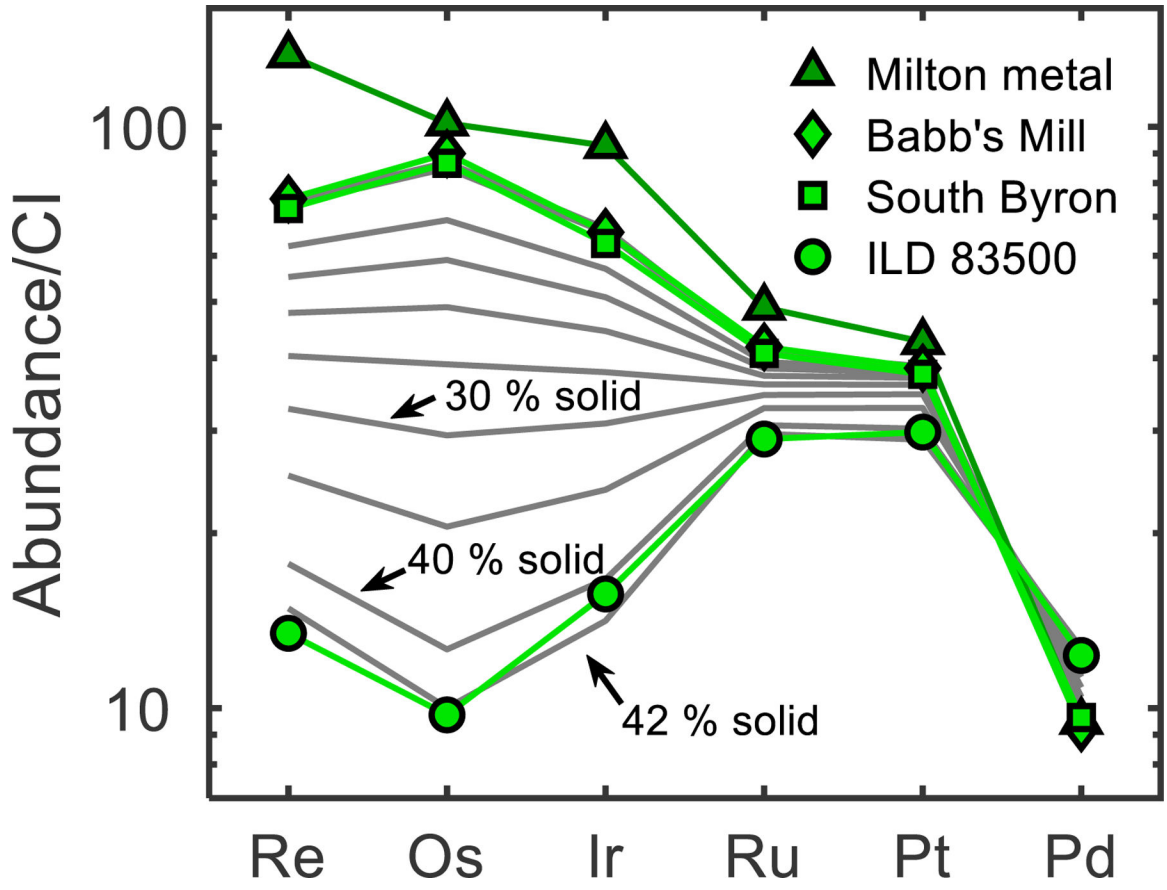

Fig. 4.

CI-chondrite normalized HSE contents of Milton and the SBT, and HSE abundance results of a fractional crystallization model (grey lines). Babb's Mill, South Byron and ILD 83500 match 1 %, 2 %, and 42 % metal crystallization in this model, respectively. Model results are shown for 10 % to 40 % solid in 5 % increments, as well as the 1 %, 2 %, and 42 % model matches to the SBT. Model results for 1 % and 2 % are covered by patterns for Babb's Mill and South Byron.

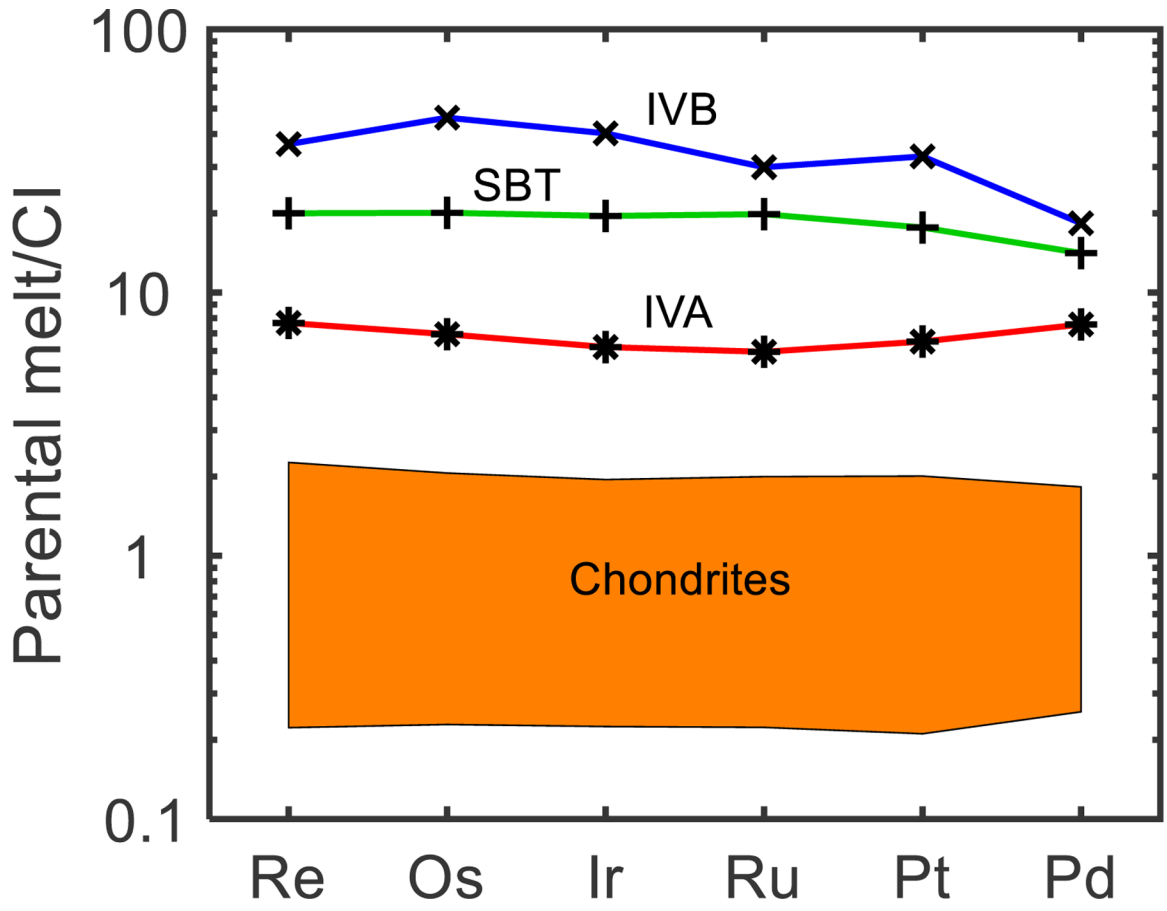

Fig. 5.

CI-normalized calculated HSE parental melt composition of the SBT, assuming 7 wt. % S, 1 wt. % P, and <0.05 wt. % C. Also shown are CI-normalized calculated parental melt compositions for the IVA irons (McCoy et al., 2011), IVB irons (Walker et al., 2008), and the range of HSE concentrations in chondrites (Horan et al., 2003; Fischer-Gödde et al., 2010).

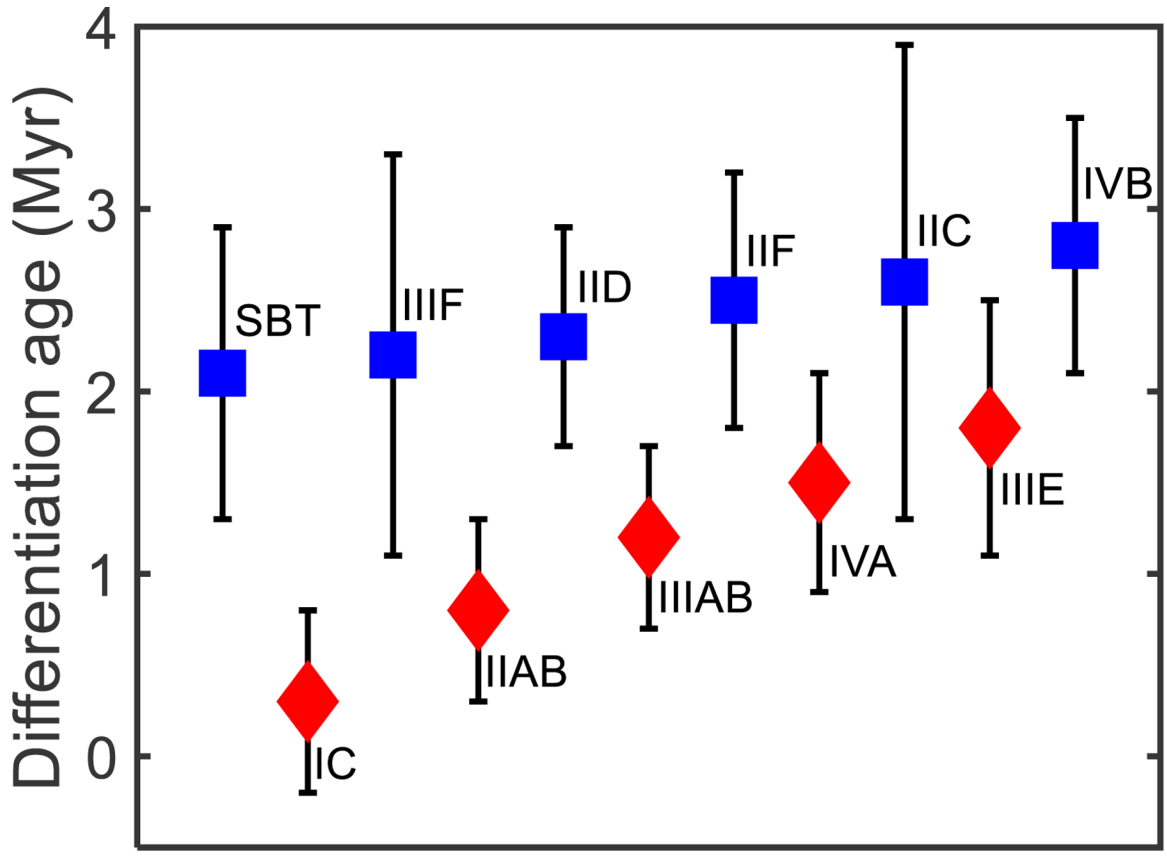

Fig. 6.

Tungsten model metal-silicate differentiation ages (post CAI formation in Myr) in ascending order of ages for the SBT parent body compared to data for other CC type (blue) and NC type (red) bodies from Kruijer et al. (2017). The SBT has a W model age that overlaps with the other CC type bodies and most NC type bodies, within uncertainty.

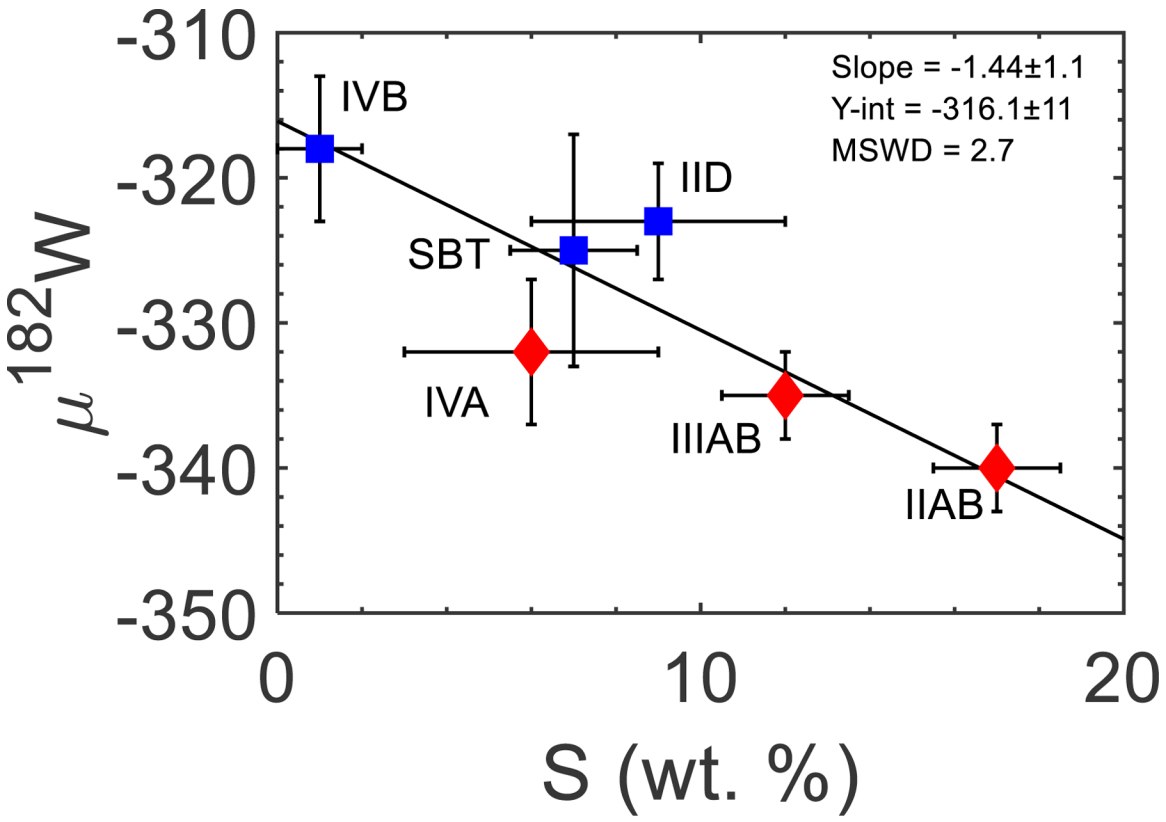

Fig. 7.

Parental melt S content *vs.* $\mu^{182}W_{Corr}$ values. The IIAB, IIIAB, IVA, IID, SBT, and IVB irons define a single trend. Sulfur contents are from Chabot (2004) and Goldstein et al., (2009), and $\mu^{182}W$ values are from Kruijer et al. (2017).

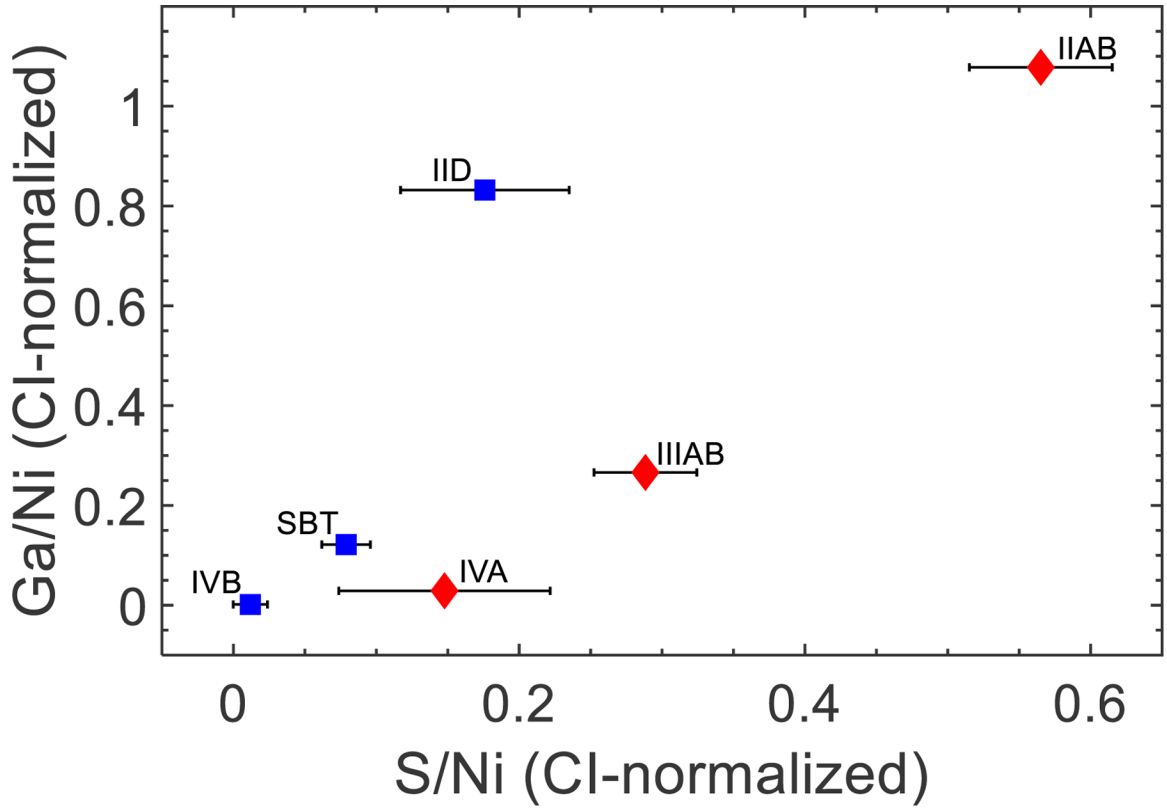

Fig. 8.

S/Ni (CI-normalized) *vs.* Ga/Ni (CI-normalized) plot for the IIAB, IIIAB, IVA, IID, SBT, and IVB irons. Blue symbols are CC bodies and red symbols are NC bodies. There are two distinct trends observed for the NC and CC bodies, suggesting that the CC parental melts have an additional S depletion not observed for NC parental melts. Since the offset is not observed for Ga concentrations, the depletion in S for CC parental melts relative to NC parental melts is likely not due to volatile depletion.

Table 1

Molybdenum and Ru isotopic compositions of Milton, the SBT, and the average value of the SBT parent body.

Sample	n[a]	μ^{94}Mo	±	μ^{95}Mo	±	μ^{97}Mo	±	n[a]	μ^{100}Ru	±
Milton	2	+130	26	+104	9	+54	5	3	−114	15
Babb's Mill	5	+132	9	+104	5	+46	3	2	−104	9
South Byron	4	+127	12	+104	6	+50	3	3	−111	9
ILD 83500	4	+121	13	+99	9	+50	2	3	−104	10
SBT average	13	+127	7	+103	4	+49	2	8	−107	5

[a] n is the number of analyses for Mo and Ru isotopic composition. The reported isotopic values reflect the average values obtained for each meteorite piece. Uncertainties reflect the largest (of n analyses) 2SD of the standards run during an analytical campaign (n ≤ 3) or 2SE (n > 3) of the sample values.

Table 2

Tungsten isotopic compositions of the SBT.

Sample	n[a]	$\mu^{182}W_{Measured}$	±	$\mu^{183}W_{Measured}$	±	$\mu^{182}W_{Corrected}$	±	ΔT_{CAI}	±
Babb's Mill	1	−307	6	+11	6	−323	10	2.3	1.0
Babb's Mill (*rep*)	1	−312	6	+4	7	−318	12	2.8	1.2
South Byron	1	−311	6	+15	6	−332	10	1.4	0.9
ILD 83500	1	−319	6	+7	6	−329	10	1.7	1.0
SBT average	4	−312	5	+9	5	−325	8	2.1	0.8

[a] n is the number of analyses. The measured $\mu^{182}W$ and $\mu^{183}W$ values are reported for each meteorite piece and the uncertainties reflect the 2SD of the standards run during an analytical campaign. The corrected $\mu^{182}W$ represents the value corrected for the $\mu^{183}W$ positive anomaly per sample, where $\mu^{182}W_{corrected} = \mu^{182}W_{Measured} - (1.41\pm0.06*\mu^{183}W)$ (Kruijer et al., 2014a), and the uncertainties reflect the uncertainties from $\mu^{182}W_{Measured}$, $\mu^{183}W_{Measured}$, and the $\mu^{183}W$ correction. The SBT average $\mu^{182}W_{Corrected}$ values were calculated using the SBT average $\mu^{182}W_{Measured}$ and $\mu^{183}W_{Measured}$ values, and errors represent 2SE. The ΔT_{CAI} ages were calculated from the $\mu^{182}W_{Corrected}$ values.

Table 3

Rhenium-Os isotopic and HSE composition data for Milton and the SBT.

Sample	Wt.	Ni	Re	Os	Ir	Ru	Pt	Pd	$^{187}Re/^{188}Os$	$^{187}Os/^{188}Os$	$^{\Delta}Os$
Milton Metal	0.011	15.0	5052	46554	42260	31840	36620	5338	0.5237	0.13711	+3.9
Babb's Mill	0.051	17.7	2858	41286	29990	27250	32990	5205	0.3332	0.12177	+0.8
South Byron	0.053	17.8	2750	39741	28690	26550	32200	5422	0.3332	0.12174	+1.1
ILD 83500	0.147	17.5	511.5	4470.0	7159	18910	25610	6934	0.5522	0.13897	−0.1

Samples are listed in order of descending Re concentration. Units of sample weight are in g. Nickel concentrations are given in wt. % as compiled from Scott et al. (1973), Wasson et al. (1989), and Jones et al. (2003). All other concentrations were determined by isotope dilution and are reported in ng/g. The uncertainties for $^{187}Re/^{188}Os$ ratios are ±0.15 %, the uncertainties for $^{187}Os/^{188}Os$, and Os and Re concentrations are ±0.1 %, and the uncertainties for Ir, Ru, Pt, and Pd concentrations are <2 %. Δ is the deviation of $^{187}Os/^{188}Os$ of a sample from a primordial isochron in units of per mil, with an uncertainty of ±2 per mil (Cook et al., 2004). A primordial isochron was calculated using a Solar System $^{187}Os/^{188}Os = 0.09531$, present day chondritic $^{187}Os/^{188}Os = 0.1270$ and $^{187}Re/^{188}Os = 0.40186$, and $\lambda = 1.666 \times 10^{-11}$ yr^{-1} (Smoliar et al.,1996; Shirey and Walker, 1998).

Table 4

Parental melt compositions calculated for HSE, S, P, and C for the best-fit model to reproduce the SBT chemical patterns, and comparison to IVA and IVB systems.

	Re	Os	Ir	Ru	Pt	Pd	S	P	C
SBT parental melt	770	9400	8500	13000	16000	8400	7	1	<0.05
IVA parental melt[a]	295	3250	2700	3900	5900	4500	3	0.1	0
IVB parental melt[b]	1410	21600	17500	19600	29800	10900	2	0.65	0

Concentrations are in ng/g for HSE and wt. % for S, P, and C.

[a]From McCoy et al. (2011).

[b]From Walker et al. (2008).

Table 5

Model accretion ages for NC and CC type iron meteorites determined using the thermal model described in the supplementary materials.

Iron meteorite group	Differentiation age ± 2σ (Myr)	Accretion age (Myr)
NC type		
IC	0.3 ± 0.5	0.3 ± 0.3
IIAB	0.8 ± 0.5	0.5 ± 0.5
IIIAB	1.2 ± 0.5	0.7 ± 0.4
IIIE	1.8 ± 0.7	1.0 ± 0.5
IVA	1.5 ± 0.6	0.9 ± 0.5
CC type		
SBT	2.1 ± 0.8	1.1 ± 0.5
IIC	2.6 ± 1.3	1.2 ± 0.6
IID	2.3 ± 0.6	1.2 ± 0.4
IIF	2.5 ± 0.7	1.3 ± 0.5
IIIF	2.2 ± 1.1	1.1 ± 0.6
IVB	2.8 ± 0.7	1.4 ± 0.5

All model differentiation age data are from Kruijer et al. (2017) except for the SBT.